Available online at www.sciencedirect.com
ScienceDirect
Journal of Nuclear Materials 363–365 (2007) 1386–1394
journal of nuclear materials
www.elsevier.com/locate/jnucmat

Relation between charge exchange flux and impurity influx studied by perturbation methods of gas puffing, heat load and confinement properties in TRIAM-1M

H. Zushi [a,*], Y. Nozaki [b], R. Bhattacharyay [b], K. Nakashima [b], M. Sakamoto [a], K. Hanada [a], H. Idei [a], K. Nakamura [a], K.N. Sato [a], S. Nishi [b], M. Ogawa [b], K. Takaki [b], K. Sasaki [b], Y. Hirooka [c], M. Hasegawa [a], H. Xu [b], S. Kado [d], T. Shikama [d], S. Kawasaki [a], H. Nakashima [a], A. Higashijima [a]

[a] *RIAM, Kyushu University, Kasuga, 816-8580 Fukuoka, Japan*
[b] *Interdisciplinary Graduate School of Engineering Science, Kyushu University, Japan*
[c] *National Institute for Fusion Science, Oroshi-cho 322-6, Toki-shi 509 5292, Japan*
[d] *The University of Tokyo, Kashiwanoha 5-1-5, Kashiwa-shi 277 8582, Japan*

Abstract

A diagnostic technique to study the global structure of the recycling and impurity (molybdenum) influx from the plasma facing components is proposed and is tested using the three kinds of perturbations (gas puffing, transport oscillation, and localized heat deposition). Balmer line intensities I_{H_α}, charge exchange flux Γ_{CX} and neutral molybdenum line I_{MoI} are measured and their correlations are analyzed with response to the perturbation parameters (I_{H_α} at the gas port, density n_e, and hot spot temperature T_{hot}). A simple model calculation is done to understand these correlations. It is found that the phase reversal of Γ_{CX} with respect to n_e modulation is well reproduced and a critical density exists for the phase reversal of I_{MoI}. The evaporation Mo flux evaluated with measured T_{hot} is also compared with enhanced I_{MoI} for the heat load perturbation and it contribution to the total content of Mo ions is evaluated by ~30% increment.

PACS: 52.40.Hf; 39.30.+w; 68.43.Vx

Keywords: First wall; Recycling; Evaporation; Molybdenum; Co-deposition

1. Introduction

Experiments aiming at steady state tokamak operation SSTO have been done in TRIAM-1M ($R_0 = 0.84$ m, $a = 0.11$ m) [1]. One of our concerns with respect to SSTO is the reason why the long pulse operation has been terminated without major disruptions. In this paper we study how the plasma wall interaction PWI driven perturbation influences both recycling and impurity (molybdenum) influx among the various plasma facing components

* Corresponding author. Fax: +81 92 573 6899.
E-mail address: zushi@triam.kyushu-u.ac.jp (H. Zushi).

0022-3115/$ - see front matter © 2007 Elsevier B.V. All rights reserved.
doi:10.1016/j.jnucmat.2007.01.201

PFCs. The contribution of the typical four PFCs, such as the movable limiter ML ($\sim$0.005 m^2), the fixed poloidal limiters PL (3×0.03 m^2), divertor plates DP ($\sim$0.8 m^2) and the wall ($\sim$5 m^2), to the change in the global recycling and impurity influx is investigated. The three kinds of perturbations are considered. First, in order to simulate the problems under the situation that the enhanced recycling from the local PFC occurs, the gas puffing is modulated at a few Hz at the local position in the torus. The change in the torus structure of the recycling evaluated by hydrogen Balmer alpha line intensity ($\lambda \sim 653$ nm) I_{H_α} around the torus, the role of the modulated charge exchanged neutral hydrogen atom flux Γ_{CX} ($\sim$1 keV) on the sputtered molybdenum evaluated by the neutral molybdenum line intensity ($\lambda \sim 386$ nm) I_{MoI} are studied. Second, on the contrary, how the toroidally uniform perturbation affects the global recycling structure and Mo production is simulated by analyzing the relaxation oscillations at a few Hz between the L-mode and the enhanced current drive mode ECD [1–3]. Since this perturbation modulates density n_e and ion temperature T_i, Γ_{CX}, I_{MoI}, and I_{H_α} are modulated simultaneously. Finally, the local heat load effects on the recycling and Mo influx are studied by depositing the high heat flux of several tens of MW/m^2. In order to study the local effect the heat load deposition is adjusted by positioning the ML.

2. Experimental apparatus and diagnostics

In TRIAM-1M, the in-vessel PFCs are all metals. ML, PL, DP are made of molybdenum and wall is stainless steel. Since no iron–nickel–chromium lines are observed except for the off-normal events [3,4], it is considered that the surface of the wall is covered by a thin Mo film [5]. By adjusting the ML vertically into the plasma most dominant PWI location could be modified from ML to PLs or vice versa in the limiter configuration.

Several diagnostics are used to analyze the change in the global structure of the recycling, main process for impurity production and the role of the PFCs. An H_α measurement system is used to measure toroidal (seven positions) and poloidal (seven vertical chords along the major radius) distributions. The contributions from the ML, PL, DP and wall can be deduced from this system. In addition to this, seven spectrometers are used to study MoI and Balmer series directly viewing at the ML, DP, and the wall. The content of the Mo ions is monitored by the Mo XIII line ($\sim$34 nm). The CX flux is measured with multi point neutral particle energy analyzers. Since one of the eight viewing chords is identical to that of the MoI measurement at the different torus position, a time correlation between Γ_{CX} and I_{MoI} with respect to the sputtering process on the DP is analyzed. With the assumption of the blackbody emission the hot spot temperature T_{hot} on the ML is deduced by analyzing the continuum spectrum measured with a spectrometer in the range of 900–1600 nm. The evaporation process for Mo is studied by comparing the theoretical evaporation flux derived from T_{hot} with I_{MoI} directly viewing the ML. In addition to this the local enhanced recycling is also studied [6]. The arrangement of these diagnostics is shown in Fig. 1.

The experimental conditions are as follows: $B_t = 6$–7 T, $P_{rf} = 10$–20 kW for 2.45 GHz and 40–300 kW for 8.2 GHz (along with ECH power), $n_e = 0.1$–4.0×10^{19} m^{-3}. The gas puff modulation is done at the bottom of the chamber at the port #7 and self relaxation oscillations are found to be triggered when the rf power is just below the threshold power of the enhanced current drive mode [1–3]. These modulation frequencies are a few Hz, which is much lower than the inverse of transport time scale ($\sim$5–10 ms). The heat load effects are investigated in ECH or ECCD or bi-directional LHW experiments [7]. In these experiments escaped energetic electrons are lost mainly on ML and localized heat deposition makes a 'hot spot' on ML. Since T_{hot} increases up to the melting temperature in several seconds, the response to the localized heat load perturbation can be studied.

3. Experimental results

3.1. Gas puff modulation

Fig. 2 shows modulation results for n_e, I_p, I_{H_α} at various toroidal positions, Γ_{CX} and I_{MoI} at DP. Since the maximum amplitude of I_{H_α} is found at the gas port, this is used as the reference of the phase correlation. This perturbation causes $\Delta n_e/n_e$ of $\sim$20%. A change in the recycling structure indicates that puffed H atoms diffuse with a characteristic velocity ($\leqslant$25 m/s) within the toroidal length of $\sim$0.6 m near the gas port, and constant phase delay of H_α at further distance is found. This velocity characterizing diffusion is much less than the kinetic energy of dissociated atomic hydrogen ($<\sim$3 eV). The modulation in I_{H_α} at further location is mainly attributed to the edge density with a constant time

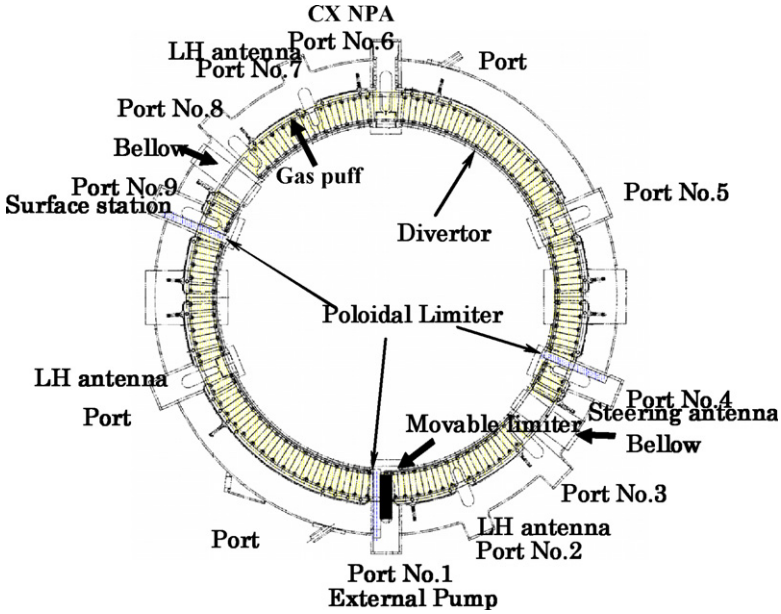

Fig. 1. Top view of the main chamber. Three PLs are installed around the torus at No. 1, 4, and 9 ports. The ML is located at No.1. The DP consisting of 8 parts is located in the inner-bottom side in the chamber and is almost toroidally uniformly installed. The H_2 gas is fed from below of the torus at No. 7. The radial profile of H_α intensity I_{H_α} is measured at No.1, 2, 3, 5, 6, 7 and 9, and the poloidal one at No. 2, 5. MoI is monitored at No. 1, 2 and 5 and MoXIII at No.8. The CX flux is measured at No. 6. IR spectrometer and CCD camera are set at No. 1.

delay of 30 ± 10 ms. I_{H_α} is modulated, however, within 10° along the major radius (± 0.1 m) and this phase relation is independent of the toroidal location. Thus injected H_2/H are considered to be diffused as neutral near the gas port with a velocity of <25 m/s and a new recycling structure is established through slow diffusion process near the gas port and fast ionization relaxation process around the torus. On the other hand, the phases of Γ_{CX} at $E \sim 1$ keV and I_{MoI} at DP are ~170° and ~100°, respectively. The amplitude of I_{MoI} variation is ~10%, but that in Γ_{CX} is higher by the order of magnitude, because of the sensitivity of Γ_{CX} on T_i. Since the density increment might lead to reduce Γ_{CX} because of both reductions in T_i and the edge neutral density, it is expected that sputtered Mo atoms are reduced. This point will be discussed in Section 4 with a simple model calculation.

3.2. Self relaxation oscillation driven by transport improvement

In order to obtain the relaxation oscillations the rf power is set just below the threshold power level [1]. After a transition from the L-mode (~40 kA), the driven current oscillates from ~43 kA (high level in L-mode) to ~48 kA (low level in ECD mode). Fig. 3 shows modulation results for n_e, I_p, I_{H_α} (inner, center and outer) along the major radius, Γ_{CX} and I_{MoI} at DP. In this case the current modulation precedes the density modulation, suggesting that the enhancement in the current drive efficiency is first triggered and then the particle confinement is improved. T_i is also self-modulated by improvement in ion energy transport. This type of modulation is considered to be the toroidal uniform modulation compared with the local perturbation in the first case. The toroidal recycling structure monitored by toroidal H_α signals is delayed by 0.1–0.2 s with respect to the start time of the density rise, but the phase relation is in phase. On the other hand the poloidal structure shows an in-out asymmetry and the radial profile of the modulation amplitude is hollow. This might be attributed to the enhanced recycling near the inner and outer edge caused by in-out shift of the plasma column. On the other hand, the phases of Γ_{CX} at $E \sim 1$ keV and I_{MoI} are ~0 and ~140° with respect to n_e, respectively. The amplitude of I_{MoI} variation is ~10%, but that in Γ_{CX} is ~200%.

3.3. Heat load perturbation by adjusting the ML

Fig. 4 shows the time evolution of the I_{MoI} at the ML, DP and wall when the additional heat load is

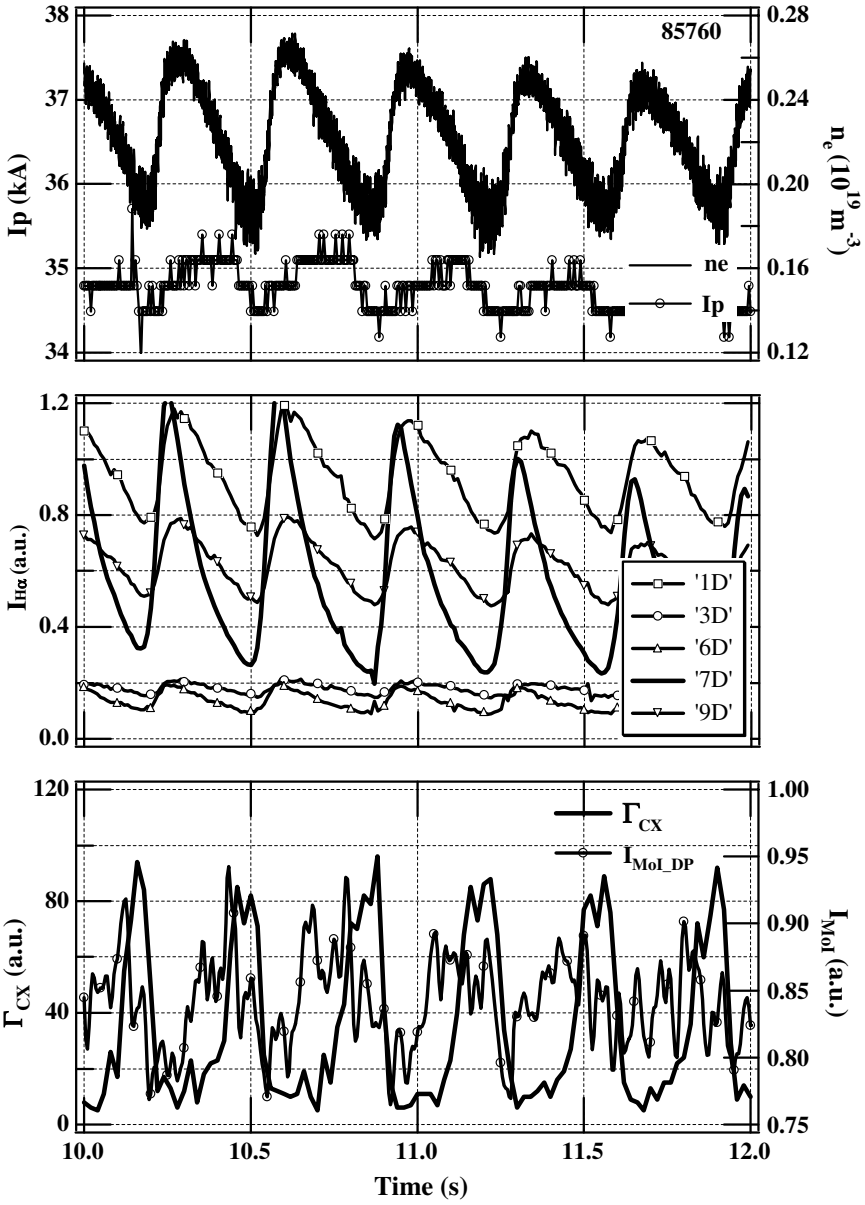

Fig. 2. Example of modulations in n_e, I_p, I_{H_α} at several toroidal positions, Γ_{CX}, I_{MoI} for gas puff modulation. Gas is fed at #7 port, Γ_{CX} at #6 port and I_{MoI} at #2 port. All H_α signals are taken at R_0.

deposited on the ML. The hot spot temperature is evaluated by the spectrum analysis. The contribution of the Mo source influx from PFCs to the total content of Mo ions is deduced from comparison with I_{MoXIII}. The enhanced local interaction with ML by adjusting the position causes this to be the dominant source position for Mo. Actually, I_{MoI} at ML is abruptly increased and it is deduced from 10 s to 30 s from the evolution of the intensity I_{IR} in the infrared spectrometer at $\lambda = 1\,\mu m$ that T_{hot} on ML is abruptly raised. Since the emission in the infrared region is dominated by the black body emission, the I_{IR} is very sensitive to the hot spot temperature formed on the ML. However, I_{MoI} from DP shows no enhancement and I_{MoI} from wall at port #5 is also remained constant. Thus, it is considered that localized interaction with particular PFC only causes the local impurity source. Especially, for 13–19 s I_{MoI} at ML is kept high level and this peak value of I_{MoI} is 10 times higher than the previous level which may be caused by sputtering. The density is increased by 20% for this phase, and the MoXIII intensity is also

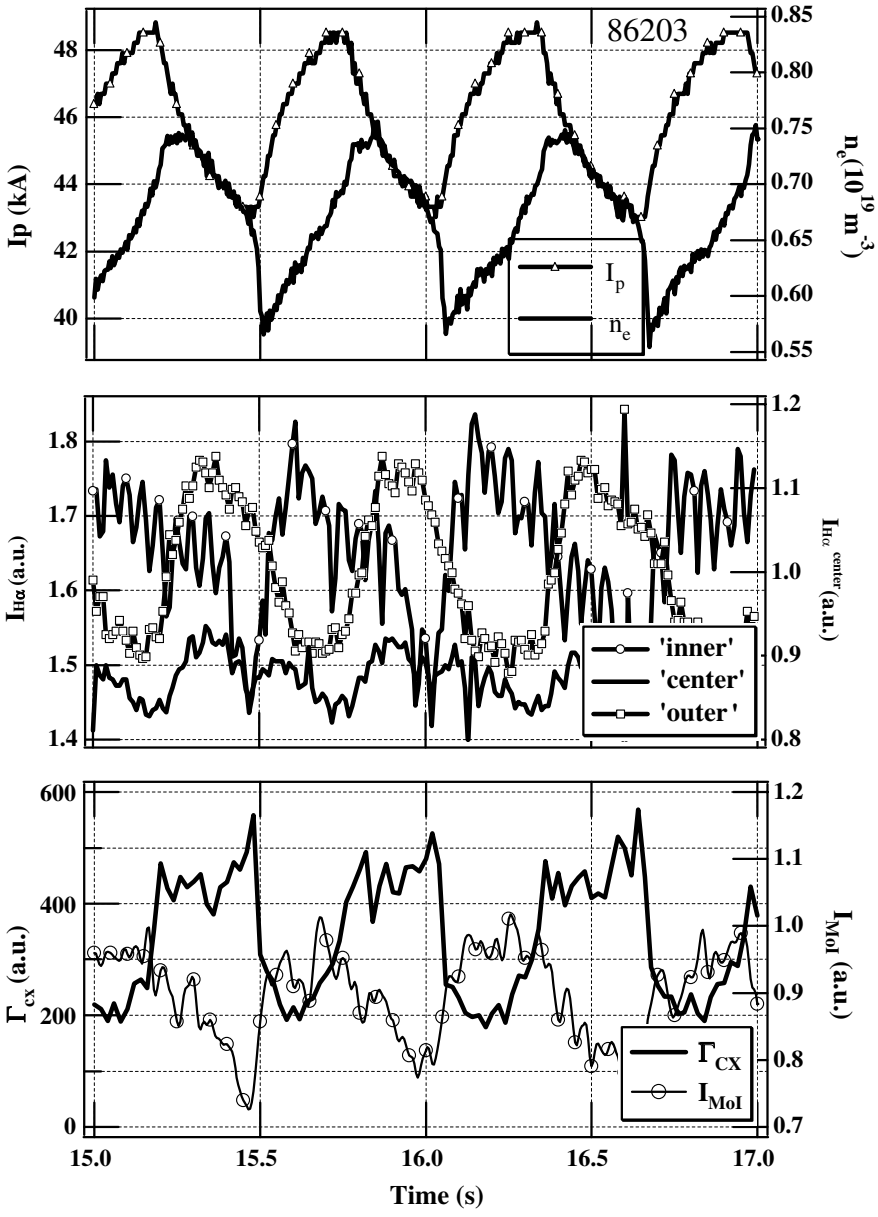

Fig. 3. Example of modulations in I_p, n_e, I_{H_α} at poloidal positions, Γ_{CX}, I_{MoI} for relaxation oscillation. The Γ_{CX} is taken at #6 port and I_{MoI} at #2. At #9 port I_{H_α} are taken along the inner, center and outer chords.

raised by <30%. Detailed comparison of I_{MoI} at ML with T_{hot} will be discussed in Section 4.2.

4. Discussion

4.1. Model calculation of the phase relation between Γ_{CX} and I_{MoI}

In order to understand the correlation of Γ_{CX} and I_{MoI} with respect to the gas modulation, a model calculation is performed. The profiles of n_e, n_i, T_e, and T_i are assumed parabolic ones, and the neutral particle density profile $n_0(r)$ is assumed to be $n_0(r) = n_0(a)\exp\left(-\int_a^r n_e(r)\bar{\sigma}_{ion}\,dr\right)$, here $\bar{\sigma}_{ion}$ is the rate coefficient of electron impact ionization for atomic hydrogen with $E = 3$ eV and a is the radius of the plasma. In this calculation $n_0(a)$ is fixed and density is modulated. Thus model equations for $\Gamma_{CX}(E = 1\,\text{keV})$ and I_{MoI} are as follows:

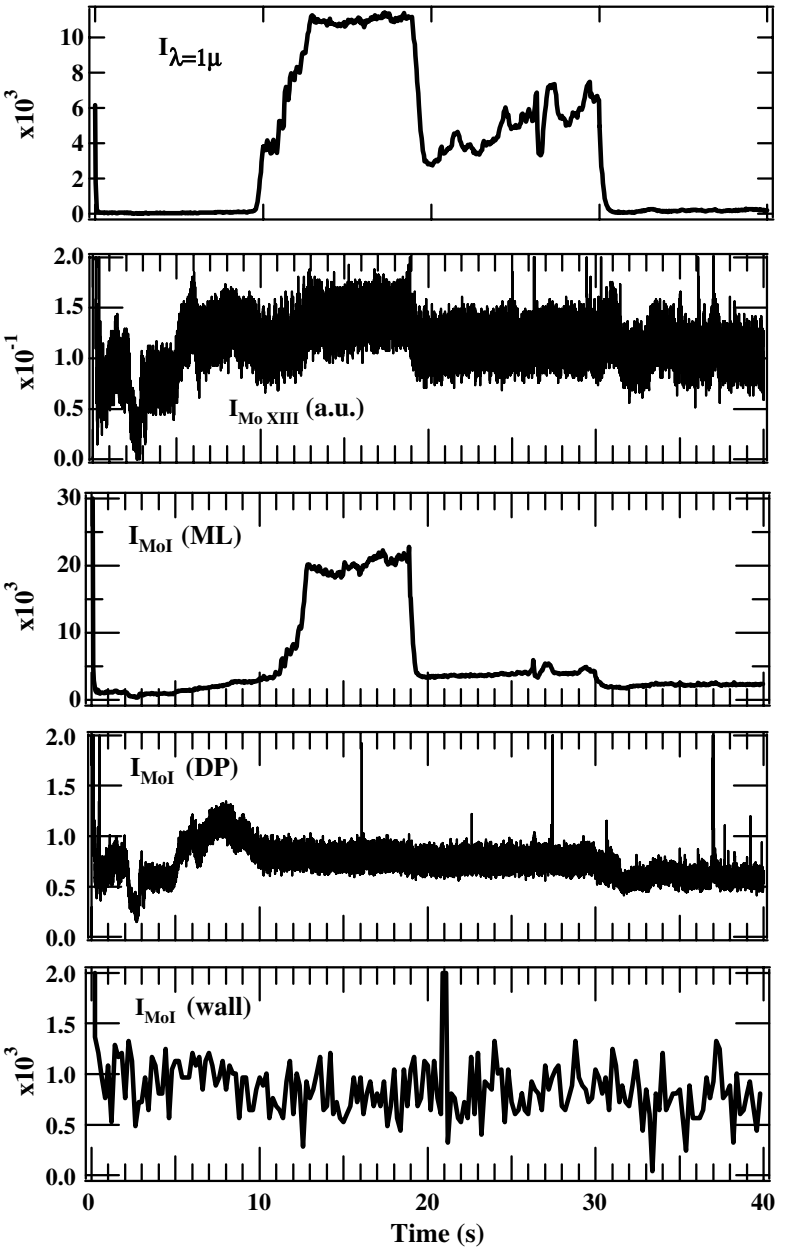

Fig. 4. Evolution of I_{ir} at $\lambda = 1$ μm, I_{MoXIII}, I_{MoI} at ML, DP, and wall in a discharge with local heat deposition on the ML.

$$\Gamma_{CX}(E) = \int_{-a}^{a} dr n_i(r) n_0(r) f_M(T_i, E) \sigma_{CX}(E) E \exp\left(-\int_r^a \frac{dl}{\lambda_{mfp}}\right),$$

$$I_{Mo} = \int_{-a}^{a} dr n_e(r) n_{Mo}(a) \langle \sigma v \rangle_{exc} \exp\left(-\int_a^r \frac{dl}{\lambda_{ion}}\right),$$

$$n_{Mo}(a) = Y(E)\Gamma_{CX}(E)/v_{sp},$$

where $\lambda_{ionH} = v_0/n_e \langle \sigma v \rangle_{ionH}$ and $\lambda_{ionMo} = v_{sp}/n_e \langle \sigma v \rangle_{ionMo}$ are ionization mean free paths of H and Mo with an assumption of incident energy of 3 eV and 4.5 eV, respectively, $\langle \sigma v \rangle$ their rate coefficients, f_M Maxwell energy distribution function, σ_{CX} the CX cross section, $\langle \sigma v \rangle_{exc}$ the excitation rate coefficient, $Y(E) \sim 10^{-3}$ the sputtering yield, v_{sp} the averaged velocity of the sputtered Mo. For the gas modulation the $n_e(0)$ is only modulated at 2 Hz with keeping the profile constant. $\Gamma_{CX}(t)$ is simulated to be out of phase with respect to the phase of $n_e(t)$ because the attenuation factor $\left(\propto \exp\left(-C \int_r^a n_e(t) dl\right)\right)$ dominates the product $n_i(t) n_0(t)$. The neutral density $n_0(t)$ has also a similar

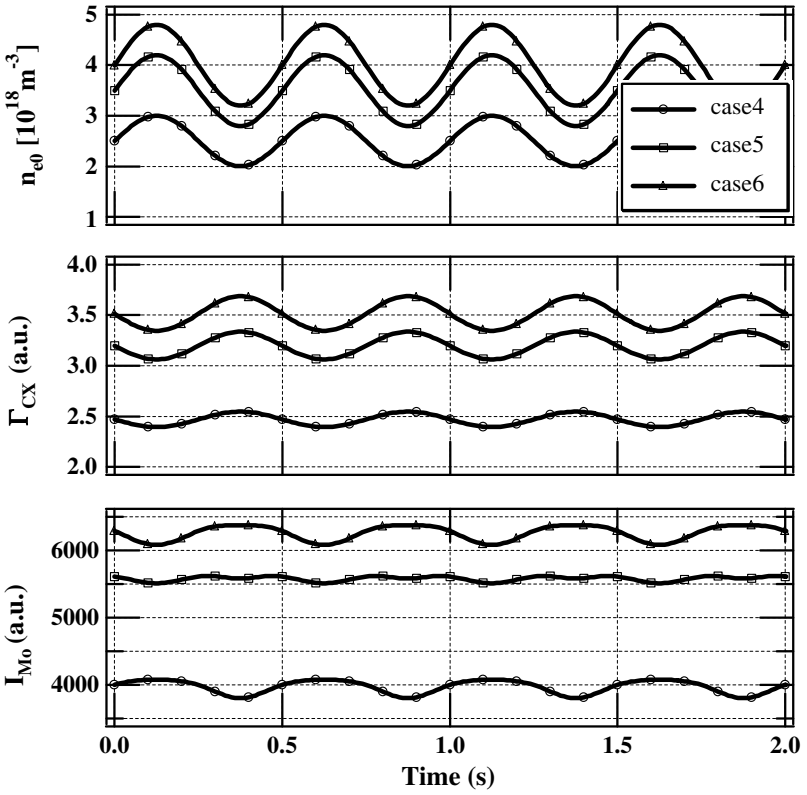

Fig. 5. The results of model calculation for n_e, Γ_{CX} and I_{MoI} for gas puff modulation. $n_e(0)$ is varied from 2.5×10^{18} m^{-3} to 4×10^{18} m^{-3}. A clear phase reversal of I_{MoI} is found.

factor $\left(\propto \exp\left(-C'\int_a^r n_e(t)\mathrm{d}l\right)\right)$. The incident Mo density $n_{Mo}(a)$ is modeled by the H sputtered flux and $I_{Mo}(t)$ is calculated by taking into account the attenuation of incident Mo atom, $\exp\left(-\int_a^r \frac{\mathrm{d}l}{\lambda_{ion}}\right)$. Thus the phase of $I_{Mo}(t)$ depends on $n_e(t)$, $n_{Mo}(a;t)$ due to $\Gamma_{cx}(t)$ and ionization loss due to path integration of $n_e(t)$. The phase of $I_{Mo}(t)$ is simulated to be in phase when $n_e(0) < n_e^* = 0.35\times10^{19}$ m^{-3} and become out of phase for $n_e(0) > n_e^*$, shown in Fig. 5. Here n_e^* is a critical density. Although the ionization factor has an intrinsic out of phase property, the phase reversal is not calculated in this density range when $n_{Mo}(a)$ is modeled constant. Thus it is considered that the sputtering process is essential to the phase relation of I_{MoI} [8,9]. The experimental 100° phase different may be reasonably explained. For the transport oscillation, $T_i(0)$ (=400 eV) is also modulated by 20% in phase as n_e. On the contrary of the gas puffing simulation, both $\Gamma_{CX}(t)$ and $I_{Mo}(t)$ behave similarly in phase and no density dependence of the modulation phase is found in the range from 0.15×10^{19} to 1.5×10^{19} m^{-3}.

4.2. Mo influx due to evaporation

At $t = 9$ s T_{hot} starts to increase and reaches ~2900 K (= Mo melting temperature) at $t = 13$ s, and is kept above 2200 K for ~6 s, as shown in Fig. 6. Although T_{hot} is kept ~2000 K until 30 s, I_{MoI} is reduced to the original level. There seems that a critical temperature (~2200 K) exists above which the evaporated Mo flux Γ_{Mo}^{eva} overcome the sputtered Mo flux. According to the intensity ratio of the absolutely measured one to the black body intensity evaluated by T_{hot} the fraction of the hot spot area to the total viewed area is deduced. It is shown that a relative size of the hot spot does not follow the temperature evolution.

Following $\Gamma_{Mo}^{eva} = \exp(C)/M/\sqrt{T_{hot}}\exp(-B/T_{hot})$ [10] with numerical constants $B = 30.85\times10^3$, $C = 8.40$, atomic mass $M = 94.94$ and temperature T_{hot} in Celsius, the time evolution of the Γ_{Mo}^{eva} is derived. The comparison with the observed enhancement in I_{MoI} is quit well, as shown in figure.

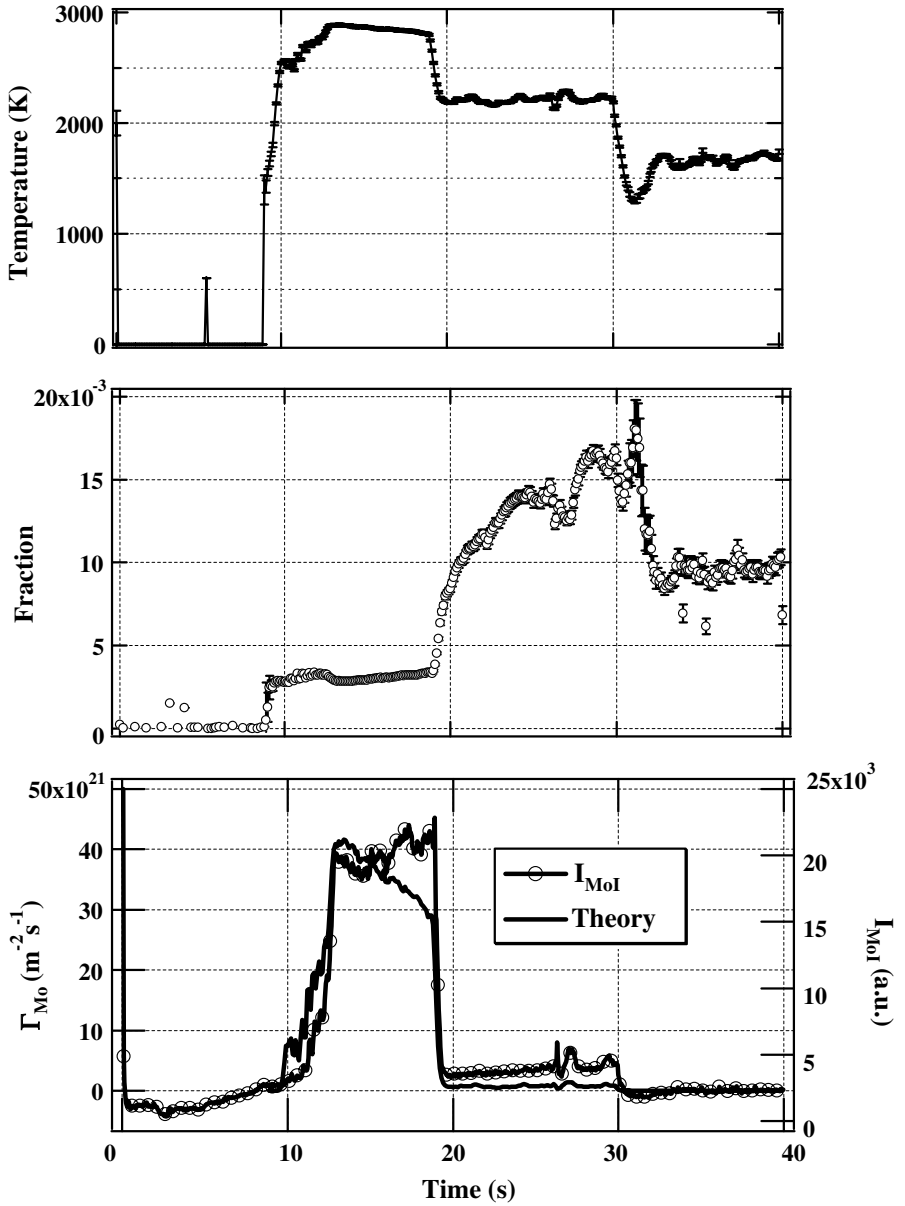

Fig. 6. Evolution of T_{hot}, the relative fraction of "hot spot" and theoretically calculated evaporation flux Γ^{eva}_{Mo}. I_{MoI} is compared with Γ^{eva}_{Mo}.

5. Conclusion

In order to investigate the role of PFCs on the global structure of the recycling and the contribution of the sputtering process by charge exchange flux on Mo influx, a new technique has been developed by combination of the perturbation at a few Hz. Since the most dominant PFC for Mo emission has been known to be DP [1], the correlation between Γ_{CX} and I_{MoI} whose line of sight is viewing at DP has been compared. The phase of Γ_{CX} is out of phase to the phase of n_e for low density (0.2×10^{19} m^{-3}) gas modulation, but in-phase for relaxation oscillations at higher density ($\sim 0.8 \times 10^{19}$ m^{-3}). On the other hand, the phase of I_{MoI} is $\sim 100°$ and $\sim 140°$, respectively. A simple model calculation is done to understand these correlations and the phase of Γ_{CX} is well reproduced by taking the electron density effect on the attenuation along the path into account. It is found that a critical density exists for the phase reversal of I_{MoI}. A complete interpretation for the phase difference between Γ_{CX}

and I_{MoI} is left for future. For the heat load perturbation, the enhanced Mo influx from the ML is observed. The evolution of I_{MoI} can be well explained by the evaporation flux and a factor of ten enhancements in I_{MoI} with respect to the sputtered Mo level form ML is found to contribute to the intensity I_{MoXIII} increment by 30%.

Acknowledgement

This work is partially supported by a Grant-in-Aid for Scientific Research from Ministry of Education, Science and Culture of Japan. This work has been partially performed under the framework of the bi-directional collaboration organized by NIFS.

References

[1] H. Zushi et al., Nucl. Fusion 45 (2005) S142.
[2] H. Zushi et al., Nucl. Fusion 41 (2001) 1483.
[3] H. Zushi et al., Nucl. Fusion 43 (2003) 1600.
[4] T. Kuramoto, H. Zushi, et al., in: 30th EPS, vol. 27A, St. Petersburg, 2003, P2125.
[5] K. Sasaki, K. Hanada, et al., in: 17th PSI Conference, 2006, P1-27.
[6] R. Bhattacharyay, H. Zushi, et al., J. Nucl. Mater., these Proceedings, doi:10.1016/j.jnucmat.2007.01.117.
[7] H. Zushi et al., in: Proceedings of 14th Workshop on ECE and ECRH, Santorini, 2006, p. 96.
[8] T. Hirai et al., J. Nucl. Mater. 290–293 (2001) 94.
[9] N. Yoshida et al., J. Nucl. Mater. 290–293 (2001) 1030.
[10] R. Behrisch et al., J. Nucl. Mater. 93&94 (1980) 498.